Mercury(II) Adsorption from Wastewaters Using a Thiol Functional Adsorbent

Kwan H. Nam, Sergio Gomez-Salazar, and Lawrence L. Tavlarides*

Department of Chemical Engineering & Materials Science, Syracuse University, Syracuse, New York 13244

The removal of mercury(II) from wastewaters (coal-fired utility plant scrubber solutions) using a thiol functional organoceramic composite (SOL-AD-IV) is investigated. A simulant is employed as a surrogate to demonstrate the removal of mercury from real waste solutions. Equilibrium studies show a mercury uptake capacity of 500 mg/g at a low mercury concentration of 0.5 mg/L and 726 mg/g at saturation. Adsorption is observed to be independent in the pH range 3−5. The kinetic performance assessed on a recycle batch reactor shows a rapid rate of adsorption. Selectivity is found to be in the order Hg(II) > Pb(II) ∼ Cd(II) > As(V) > Cr(III). Regeneration of SOL-AD-IV is accomplished using 12 M HCl. Effluent mercury concentrations of <0.001 mg/L are achieved using a fixed-bed adsorption column. A stability test operated for 25 cycles indicates a capacity loss of <10%. A high potential is demonstrated for application for mercury cleanup of wastewaters.

1. Introduction

The extreme toxicity of mercury poses a serious threat to the environment. Discharge of mercury from industries and thereby the contamination of waters have brought global concerns to environmental authorities. Cleanup of wastewaters is essential prior to discharge. Recently, attention has been focused on the fate of mercury from coal-fired utility plants, including mercury containing flue gas scrubber waters. Wet scrubbers are common flue gas cleanup methods. The United States Environmental Protection Agency (USEPA) and Electric Power Research Institute (EPRI) estimate that coal-fired utility commercial boilers emit 50−55 tons of total mercury per year in the U.S.[1] The scrubber waters consist of approximately 0.5 mg/L (500 μg/L) mercury(II) at a pH near 5.[1,2] The permitted discharge limit of wastewater for total mercury is 10 μg/L,[3] and the EPA water-drinking limit is 2 μg/L.[4] An environmentally sound and cost-effective mercury control technology is required to meet and exceed these limits.

Numerous separation processes have been applied for effectively reducing mercury concentrations from various aqueous solutions, including ion exchange,[3,5−15] solvent extraction,[16−22] adsorption,[23−27] precipitation,[28,29] and membrane separation.[30,31] Although traditional solvent extraction processes have been widely utilized, they have less applicability toward dilute solutions and are economically infeasible because of the loss of solvents after use. Ion-exchange resins can remove metal ions substantially; however, they do not show mechanical strength, due to swelling of the polymeric skeleton, and low selectivity. Many chelating resins have been reported but show limited applicability because of their poor hydrophilicity, small surface area, slow rate of adsorption, and lack of regenerability.[32] Adsorption, on the other hand, is a conventional technique, and by using functionalized adsorbents of inert backbone such as ceramics, the drawbacks of the former separation processes can be overcome.

Of interest are sulfur derivative functional adsorbents because of their strong affinity toward mercury. From the principle of hard and soft acids and bases,[33] mercury (a soft acid) prefers to bind with sulfur (a soft base) through covalent attachment.[34] Surface functionalizations of ceramic supports by solvent deposition and covalent attachment techniques are common synthesis methods.[35] The advantage of these methods lies on the utilization of a nonswelling and mechanically and thermally stable skeletal framework. However, these synthesis methods have limitations in maximizing ligand densities because of the availability of the hydroxyl groups on the supports and the accessibility of the hydroxyl groups in the micropores.[36] These deficiencies are overcome by applying the sol−gel synthesis technique to form a silica network with functional ligands through a liquid-phase reaction. This technique enables better control of structural properties such as pore size and surface area. Recent work[36] shows superiority of the sol−gel synthesis method over the immobilization method.

A thiol functional organoceramic adsorbent, SOL-AD-IV, developed in our laboratory for the extraction of mercury and other soft metals,[36] has been synthesized to have high ligand density, large defined pore sizes, and high surface area. The objective of this study is to demonstrate the effectiveness of the adsorbent for the reduction of the mercury concentration from scrubber waters at pH 5 containing 0.5 mg/L to sub microgram per liter levels using a scrubber water surrogate.

2. Experimental Section

2.1. Materials, Reagents, and Equipment. SOL-AD-IV is a thiol (SH) functional hydrophilic organoceramic composite synthesized by the sol−gel method. Details of the synthesis are described elsewhere.[36] The adsorbent is stored under an argon atmosphere to prevent oxidation of thiols to disulfides.

All reagents used in this study are of analytical reagent (AR) grade chemicals obtained from Aldrich and Fisher Scientific and are used as received. The functional precursor, (3-mercaptopropyl)trimethoxysilane

* To whom correspondence should be addressed. Tel.: 1-315-443-1883. Fax: 1-315-443-1243. E-mail: lltavlar@ecs.syr.edu.

10.1021/ie020834l CCC: $25.00
Published on Web 03/28/2003

Table 1. Composition of a Coal-Fired Utility Scrubber Water Matrix Simulant

ion	mg/L	mol/L	ion	mg/L	mol/L
Ca^{2+}	350	0.008 73	NH_4^+	206	0.011 44
Mg^{2+}	50	0.002 06	Cl^-	1100	0.031 02
Zn^{2+}	30	0.000 46	SO_4^{2-}	550	0.005 72
Na^+	714	0.031 04	NO_3^-	1338	0.021 58

[MPS; $(CH_3O)_3Si(CH_2)_3SH$], and the cross-linking agent, tetraethoxysilane [TEOS; $(CH_3CH_2O)_4Si$], for material synthesis are purchased from Aldrich and used as received. Stock solutions of each metal used are generated by dissolving the salts ($Hg(NO_3)_2 \cdot H_2O$, $CdCl_2 \cdot 2.5H_2O$, $As_2O_5 \cdot 3H_2O$, $Cr(NO_3)_3 \cdot 9H_2O$, and $Pb(NO_3)_2$) in 2% (by volume) nitric acid. The pH is measured with a Chemcadet pH meter. Structural properties (surface area, pore diameter, and pore volume) are measured with an ASAP 2000 automatic analyzer (Micromeritics Instrument Corp.) using ultrapure nitrogen. Ligand coverage of SOL-AD-IV is determined by elemental analysis employing an accredited laboratory (Oneida Research Services, Inc., Whitesboro, NY). A thermostatically controlled shaker water bath (Precision Scientific model 50) is used in batch adsorption experiments. Vacuum filtration is conducted using Millipore glass fiber filters (0.7 μm particle retention) to remove particulates. Analyses of the total mercury, cadmium, arsenic, chromium, and lead concentrations are conducted using inductively coupled plasma equipped with a mass spectrometer (ICP-MS ELAN 6100 by Perkin-Elmer). The analytical procedures and methods are conducted according to USEPA standard methods for metal ion analysis.

Adsorbents are conditioned in DI water overnight at the pH of interest prior to every adsorption experiment to ensure wetting of the pores. Particle sizes of 75−125 and 125−180 μm are used for batch and column (including recycle batch) experiments, respectively. The amount of metal ions adsorbed is calculated by a mass balance difference of the initial and residual solution concentrations.

2.2. Simulated Coal-Fired Utility Scrubber Solution. A coal-fired utility scrubber water simulant with the composition shown in Table 1 is prepared and used as the solution matrix of all experiments. Appropriate volumes of the mercury stock solution are spiked in the simulant matrix solution to generate desired mercury concentrations.

2.3. Adsorption Equilibrium. Equilibrium adsorption experiments are conducted at pH 3, 4, and 5 in batch modes. An adsorbent amount of 0.2 g is equilibrated with 100 mL of a mercury solution of various initial concentrations ranging from 150 to 1800 mg/L for 24 h at 25 °C. An acetate buffer of 0.1 M is used to control the pH. The reaction mixture is filtered, and the filtrate is collected for analysis of the mercury concentration.

2.4. Adsorption Kinetics. Kinetic experiments at different initial concentrations are performed in a differential recycle batch reactor.[37] Initial concentrations of mercury in the feed solution tank are set at 0.5, 5, and 50 mg/L at pH 5, each buffered by 0.1 M acetate. Mercury solutions are passed through the 1.0 cm i.d. column packed with 0.2 g of SOL-AD-IV at a flow rate of 40 mL/min and 25 °C. This flow rate is employed to minimize external mass-transfer resistances. Samples of the tank solution are taken at time intervals for analyses of the mercury concentrations.

2.5. Stripping. Stripping tests are conducted in 0.7 cm i.d. columns using three concentrations of hydrochloric acid (6, 9, and 12 M). Volumes of 500 mL of 400 mg/L mercury solutions at pH 5 are used to load the column containing 0.2 g of SOL-AD-IV. Stripping solutions of 50 mL each are used. Washings of the column using 5 mL of DI water are performed before and after stripping steps to ensure discharge of any physically bound or interstitially entrained mercury. Effluent concentrations are collected at time intervals for analyses.

2.6. Selectivity. Selectivity of SOL-AD-IV for various hazardous metals is determined by simultaneous adsorption of Hg(II), As(V), Cd(II), Cr(III), and Pb(II) under excess molar quantities of sites. Equimolar quantities of each metal (0.0744 mmol) in a 1 L solution at $pH_{initial}$ 5 are prepared for contact with 0.5 g of SOL-AD-IV for 24 h at 25 °C. The reaction mixture is filtered, and the filtrate is collected for analyses. The composition provides 20% saturation of the functional sites. This level of saturation minimizes the competition between metals for sites and permits ligand-to-metal affinities to be determined.

2.7. Fixed-Bed Column Adsorption. The column performance is tested using high and low concentrations of mercury. The high-concentration experiment consists of flowing 3.1 L of a 50 mg/L mercury solution at pH 5 at a flow rate of 1 mL/min through a 0.7 cm i.d. column packed with 0.2 g of SOL-AD-IV. The low-concentration experiment consists of flowing 205 L of a 0.5 mg/L mercury solution at pH 5 at a flow rate of 6 mL/min through a 0.7 cm i.d. column packed with 0.175 g of SOL-AD-IV. Effluent concentrations are collected at time intervals for analyses.

2.8. Stability. The stability of SOL-AD-IV for multiple adsorption/desorption cycles is tested using a 0.7 cm i.d. column packed with 0.2 g of SOL-AD-IV. Saturation of the column is conducted using 1 L of a 300 mg/L mercury solution at pH 5, and stripping, using 25 mL of a 12 M HCl solution. Washings of the column with DI water are employed after loading and stripping steps. The intent of the use of an excess volume of the stripping agent is to provide severe stripping conditions and challenge the chemical stability of the thiol groups. A total of 25 cycles is performed.

3. Theory

3.1. Aqueous-Phase Equilibrium Chemistry of Mercury. Aqueous-phase equilibrium concentrations of mercury species in the simulant matrix solution in which acetate buffer is added are evaluated using the chemical equilibrium modeling software MINEQL+.[38] The stability constants of mercury complexes with counterions that are present in the simulant used in the speciation calculations are provided in Table 2. The speciation calculations, presented as a percent of the total moles as a function of pH in the presence of acetate in Figure 1, indicate that mercury exists primarily as $HgCl_2^0$ at pH ≤ 3, $HgAc_4^{2-}$ at pH > 4.5 and both of these species between pH 3 and 4.5. During $HgCl_2^0$ adsorption, the equilibrium of mercury chloride complexes shifts toward the left side[10] of the following equation:

$$HgCl_2^0 + 2Cl^- \leftrightarrow HgCl_3^- + Cl^- \leftrightarrow HgCl_4^{2-} \quad (1)$$

Consequently, adsorptions of $HgCl_3^-$ and $HgCl_4^{2-}$ are

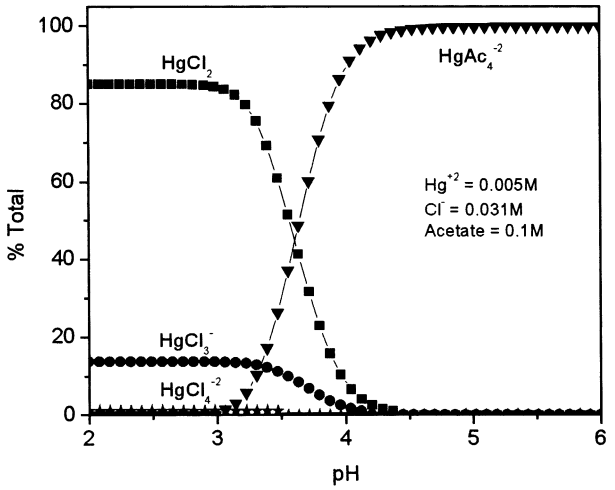

Figure 1. Speciation of mercury(II) in a scrubber matrix solution using MINEQL.

Table 2. Stability Constants of Mercury Species

reaction	log K	ref
$Hg^{2+} + Cl^- \leftrightarrows HgCl^+$	6.72	39, 40
$Hg^{2+} + 2Cl^- \leftrightarrows HgCl_2$	13.23	39, 40
$Hg^{2+} + 3Cl^- \leftrightarrows HgCl_3^-$	14.2	39
$Hg^{2+} + 4Cl^- \leftrightarrows HgCl_4^{2-}$	15.3	39
$Hg^{2+} + OH^- \leftrightarrow HgOH^+$	10.97	29
$Hg^{2+} + 2OH^- \leftrightarrows HgOH_2$	22.36	29
$Hg^{2+} + 3OH^- \leftrightarrows Hg(OH)_3^-$	21.46	29
$Hg^{2+} + Ac^- \leftrightarrows HgAc^+$	5.55	39
$Hg^{2+} + 2Ac^- \leftrightarrows HgAc_2$	9.3	39
$Hg^{2+} + 3Ac^- \leftrightarrows Hg(Ac)_3^-$	13.28	39
$Hg^{2+} + 4Ac^- \leftrightarrows Hg(Ac)_4^{2-}$	17.06	39
$Hg^{2+} + NO_3^- \leftrightarrows HgNO_3^+$	0.77	25, 39
$Hg^{2+} + 2NO_3^- \leftrightarrows Hg(NO_3)_2$	1.00	25, 39
$Hg^{2+} + SO_4^{2-} \leftrightarrows HgSO_4$	2.47	39
$H^+ + OH^- \leftrightarrows H_2O$	14	

neglected. Mercury forms weak complexes with oxyanions such as SO_4^{2-},[41] and thus their binding behaviors are neglected here. Subsequent calculations are conducted considering only the predominant mercury chloride and mercury acetate species.

Total mass balances are conducted for mercury, ligand, chloride, and acetate to be used in the subsequent model developments. Because $HgCl_2^0$ and $HgAc_4^{2-}$ are only considered here, the total mercury is the sum of these two species. The ligand balance is the sum of the unoccupied and occupied sites by the metal, where the unoccupied sites are the combination of protonated and unprotonated sites:

$$S_T = [\overline{RSH}] + [\overline{RS^-}] + [\overline{RS{\cdot}HgCl}] + [\overline{RS{\cdot}HgAc}] \quad (2)$$

where the overbars represent solid-phase species. The chloride balance consists of the sum of mercury chloride and free chloride ions, and the acetate balance consists of the sum of mercury acetate and free acetate ions.

3.2. Equilibrium Isotherm. A two-species equilibrium model is developed based on chemical reactions to describe the equilibrium phenomenon of simultaneous adsorption. Studies[6,11] have also shown that Hg(II) can form mixed ligand complexes, MLL′, at the solid phase, where M is a metal (mercury), L is a counterion (chloride or acetate), and L′ is the solid-phase functional site. Accordingly, the proposed chemical reactions of mercury chloride and mercury acetate species with thiol sites are given by

$$\overline{RSH} + HgCl_2 \leftrightarrow \overline{RS{\cdot}HgCl} + H^+ + Cl^- \qquad K_{eq1} \quad (3)$$

$$\overline{RSH} + HgAc_4^{2-} \leftrightarrow \overline{RS{\cdot}HgAc} + H^+ + 3Ac^- \qquad K_{eq2} \quad (4)$$

The expressions for equilibrium constants of reaction mechanisms (3) and (4) are

$$K_{eq1} = \frac{q_1\{H^+\}\{Cl^-\}}{[\overline{RSH}][HgCl_2]} \quad (5)$$

$$K_{eq2} = \frac{q_2\{H^+\}\{Ac^-\}^3}{[\overline{RSH}]\{HgAc_4^{2-}\}} \quad (6)$$

respectively, where $q_1 = [\overline{RS{\cdot}HgCl}]$ and $q_2 = [\overline{RS{\cdot}HgAc}]$. The appropriate activity coefficients are calculated using Davies' equation[42] and that for $HgAc_4^{2-}$ is assumed to be 1 because of the dilute concentration of interest. The concentration of deprotonated forms of thiols, $[\overline{RS^-}]$, is considered to be negligible at the working pH range of 3−5 because the pK_a of thiols on SOL-AD-IV is determined to be approximately 6.5[43] and that for the thiol ligand alone ranges from 8 to 10.[44] The site balance (eq 2) becomes $[\overline{RSH}] = S_T - q$, where $q = [\overline{RS{\cdot}HgCl}] + [\overline{RS{\cdot}HgAc}]$. The concentration of Cl^- is approximately 2 orders of magnitude greater than the sum of the mercury chloride species, and thus $Cl_T = \{Cl^-\}$. As for the acetate balance, the concentration of Ac^- is approximately 3 orders of magnitude greater than the sum of the mercury acetate species, and thus $Ac_T = \{Ac^-\}$. The total capacity, q, is defined as the sum of individual capacities of the two species in consideration $q = q_1 + q_2$. Solving for q_1 and q_2 in eqs 5 and 6 and substituting into q give the two-species equilibrium model describing the equilibrium adsorption relationship of $HgCl_2$ and $HgAc_4^{2-}$.

$$q = \frac{\left(\frac{K_{eq1}}{[H^+]\{Cl^-\}}\right)S_T[HgCl_2] + \left(\frac{K_{eq2}}{[H^+]\{Ac^-\}^3}\right)S_T[HgAc_4^{2-}]}{1 + \left(\frac{K_{eq1}}{[H^+]\{Cl^-\}}\right)[HgCl_2] + \left(\frac{K_{eq2}}{[H^+]\{Ac^-\}^3}\right)[HgAc_4^{2-}]} \quad (7)$$

For pH 3 and 5, when only one species exists and adsorbs, the above equation is simplified to

$$q = \frac{S_T K_{eq1}[HgCl_2]}{[H^+][Cl^-]\gamma_{Cl} + K_{eq1}[HgCl_2]} \qquad \text{for pH} \le 3 \quad (8)$$

$$q = \frac{S_T K_{eq2}[HgAc_4^{2-}]}{[H^+][Ac^-]^3\gamma_{Ac}{}^3 + K_{eq2}[HgAc_4^{2-}]} \qquad \text{for pH} \ge 5 \quad (9)$$

respectively. The equilibrium constants, K_{eq1} and K_{eq2}, are determined by fitting experimental data using a nonlinear regression method of Levenberg−Marquardt in Origin by Microcal.[45]

3.3. Adsorption Kinetics. Diffusion and chemical reaction rate-controlling schemes are investigated and compared to describe the adsorption kinetics. Surface diffusion and electrical potential effects are assumed to be negligible.

3.3.1. Chemical Reaction Model. The chemical reaction model is developed by considering the overall chemical reaction as the rate-limiting step. The reactor design assumes that the concentration of the solute in the reactor is approximately equal to the concentration of the feed solution tank and that the rate of reaction is constant throughout the reactor. The resulting design equation of the batch differential recycle reactor is[37]

$$-\text{rate} = \left(\frac{V_R + V_T}{V_R}\right)\frac{dC_T}{dt} \tag{10}$$

where the subscripts R and T represent the reactor and the solution tank, respectively. The adsorption rate expression derived from eq 4 is

$$\text{rate} = -\frac{d[HgAc_4^{2-}]}{dt} = k_2[\overline{RSH}][HgAc_4^{2-}] - k_{-2}[\overline{RS{\cdot}HgAc}][H^+]\{Ac^-\}^3 \tag{11}$$

Upon combining eqs 10 and 11 with appropriate mass balance substitutions, the resulting overall rate expression is solved analytically for the concentration of mercury as a function of time:

$$C(t) = \frac{De^{Ak_2} - EB}{2B - 2e^{Ak_2}} \tag{12}$$

where the constants are

$$A = \frac{V_T V_R\sqrt{F^2 - 4 - C_{b0}G}}{M(V_R + V_T)},$$

$$B = \frac{2C_{b0} + F - \sqrt{F^2 - 4 - C_{b0}G}}{2C_{b0} + F + \sqrt{F^2 - 4 - C_{b0}G}}$$

$$D = F + \sqrt{F^2 - 4 - C_{b0}G},$$

$$E = F - \sqrt{F^2 - 4 - C_{b0}G}$$

$$F = \frac{S_T M}{V} - C_{b0} + G, \qquad G = \frac{[H^+]\{Ac^-\}^3}{K_{eq2}}$$

The forward reaction rate constant, k_2, is determined by fitting eq 12 with experimental data using a nonlinear regression method of Levenberg−Marquardt in Origin by Microcal.[45]

3.3.2. Film−Pore Model. The film−pore model is developed by considering the transport of solutes through the film and pore to be rate-controlling and that the particles are of spherical geometry. The macroscopic conservation equations of the model are[46]

$$V(C_{b0} - C_b) = M\bar{q} \tag{13}$$

$$\bar{q} = \frac{3}{R_p^3}\int_0^{R_p} qr^2\, dr \tag{14}$$

where $\bar{q}$ is the mercury concentration in the pellet averaged over the pellet volume. The pore diffusion equation is

$$\left(\epsilon_p + \rho_p\frac{\partial q}{\partial C}\right)\frac{\partial C}{\partial t} = \frac{D_p}{r^2}\frac{\partial}{\partial r}\left(r^2\frac{\partial C}{\partial t}\right) \tag{15}$$

The initial and boundary conditions of the partial differential equation with the consideration of film mass transfer are given by

$$C = 0,\ q = 0 \qquad 0 \le r \le R_p \qquad \text{at } t < 0 \tag{15a}$$

$$\frac{\partial C}{\partial r} = 0 \qquad \text{at } r = 0 \tag{15b}$$

$$D_p\frac{\partial C}{\partial r} = k_f(C_b - C) \qquad \text{at } r = R_p \tag{15c}$$

where k_f is the external film mass-transfer coefficient and D_p is the pore diffusion coefficient, which are considered to be constants. D_p is defined by the conventional correlation

$$D_p = \epsilon_p D_M/\tau \tag{16}$$

where D_M and τ are the molecular diffusivity and tortuosity, respectively.

3.4. Fixed-Bed Column. The differential mass balance equation for the column neglecting axial dispersion and assuming constant superficial velocity and bed porosity is given by

$$u_s\frac{\partial C_b}{\partial z} + \epsilon_b\frac{\partial C_b}{\partial \theta} + \rho_b\frac{\partial \bar{q}}{\partial \theta} = 0 \tag{17}$$

$$C = 0,\ \bar{q} = 0 \qquad 0 \le z \le L \qquad \text{at } \theta \le 0 \tag{17a}$$

$$C_b = C_{b0} \qquad z = 0 \qquad \text{at } \theta = 0 \tag{17b}$$

where

$$\rho_b = (1 - \epsilon_b)\rho_p, \quad \theta = t - z\epsilon/u_s$$

The mercury uptake rate is given by the classical relationship involving a linear driving force across the liquid film:

$$\frac{\partial \bar{q}}{\partial \theta} = \frac{3k_f}{R_p\rho_p}(C_b - C_s) \tag{18}$$

The variable θ is the corrected time for cases when axial dispersion is negligible.[46] In this study, however, $t > z\epsilon/u_s$ because of the large time scale, and thus $\theta \sim t$.

3.5. Numerical Solution. To solve the system of partial differential equations, eqs 13−16 for kinetics and eqs 13−18 for fixed bed, the numerical method of lines (NUMOL),[47] are used. A Fortran program that has been developed for cadmium adsorption phenomena is modified and applied for this mercury adsorption study. Details on the program coding and the model development algorithm can be found elsewhere.[43]

4. Results and Discussion

4.1. Adsorbent Characterization. The results of SOL-AD-IV characterization are summarized in Table 3. Thiol coverage of 3.72 mmol/g exhibits high ligand

Table 3. Physical and Chemical Properties of the SOL-AD-IV Adsorbent

functional group	−SH
adsorbent skeleton	silica
thiol coverage density (S_T)[a]	3.72 mmol/g
BET surface area	540 ± 16 m^2/g
average pore diameter	70.3 ± 0.4 Å
pore size range	20−400 Å
pore volume	0.98 cm^3/g
pellet density[b]	0.624 g/cm^3
pellet porosity[b]	0.611

[a] Obtained from Oneida Research Services, Inc., Whitesboro, NY. [b] Calculated using correlations from ref 48.

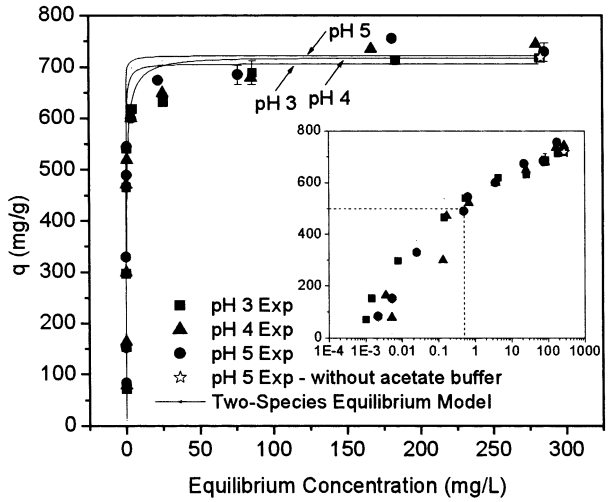

Figure 2. Adsorption equilibrium isotherms of mercury at pH 3, 4, and 5: weight of SOL-AD-IV = 0.2 g; volume = 100 mL; contact time = 24 h; buffered by 0.1 M acetate.

loading, which will provide site availability. The combined characteristics of the pore size range and large pore volume can offer sufficient ligand accessibility for transport of mercury chloride and the mercury acetate complexes with molecular lengths ranging from 4 to 5 Å. Geometrically, $HgCl_2^0$ is nearly linear at 175°, $HgAc_4^{2-}$ is tetrahedral, and the complexes have coordination numbers of 2 and 4, respectively.[41,49]

4.2. Equilibrium Isotherm. Equilibrium adsorption isotherms conducted to investigate the adsorption equilibrium behaviors and their capacities at three pH values (3, 4, and 5) in the expected range for the scrubber solution are shown in Figure 2. A high mercury uptake capacity of 500 mg/g (2.49 mmol/g) is found at the concentration of the scrubber water of 0.5 mg/L at pH 5. In the presence of acetate buffer, mercury exists as $HgAc_4^{2-}$; however, in real scrubber waters, mercury exists as $HgCl_2^0$. Thus, to investigate the effect of acetate on mercury uptake, uptake capacities of $HgCl_2^0$ and $HgAc_4^{2-}$ at equilibrium concentrations of 280 mg/L at pH 5 are compared. It is evident from the figure that the presence of the acetate buffer does not affect the adsorption capacity of mercury.

The experimentally determined equilibrium saturation uptake capacities at the investigated pH values shown in Figure 2 and the fitted equilibrium constants for mechanisms (3) and (4) are shown in Table 4. At pH 4, when the two reaction mechanisms occur simultaneously, the determined K_{eq1} and K_{eq2} values are used to fit the experimental data. The pH dependency shown, although small, over the range of 3−5 is likely due to the competition between mercury species and protons for thiol sites. The degree of this pH dependency can be explained by the strong affinity of mercury toward thiol groups. The ratios of the saturation equilibrium mercury uptake capacities and the theoretical capacity (ligand coverage density), q_{exp}/S_T, imply a 1:1 complexation mechanism between the mercury species and the thiol group.

Table 4. Fitted Equilibrium Constants

pH	q_{exp} (mmol/g)	q_{exp}/S_T[a]	K_{eq}
3	3.52[b]	0.95	$K_{eq1} = 1.4 \times 10^5$ mmol/L ± 34%
4	3.58[c]	0.96	
5	3.62[d]	0.97	$K_{eq2} = 3.8 \times 10^7$ $mmol^3/L^3$ ± 26%

[a] S_T = 3.72 mmol/g (746 mg/g). [b] 706 mg/g. [c] 718 mg/g. [d] 726 mg/g.

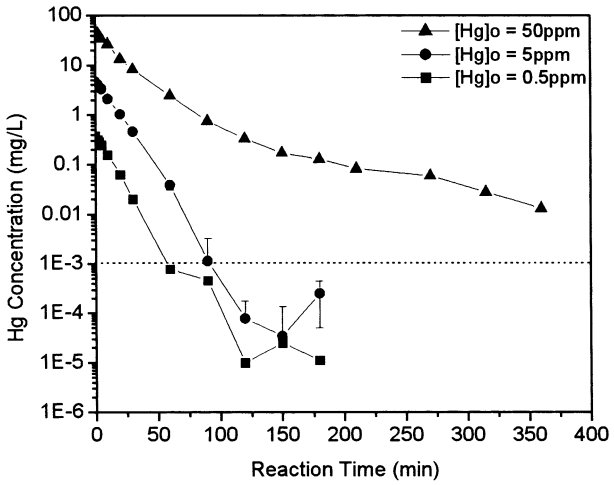

Figure 3. Adsorption kinetics of mercury for different mercury concentrations: weight of SOL-AD-IV = 0.2 g; Q = 40 mL/min; volume = 500 mL; particle size = 125−180 μm.

4.3. Adsorption Kinetics. The kinetics data of SOL-AD-IV are presented in Figure 3. The mercury concentration is rapidly reduced from 0.5 mg/L to less than 1 μg/L within 50 min of reaction time. The 1 μg/L level is illustrated with a dotted line on the figure. The scatter in data for 0.5 and 5 mg/L solutions at the lower mercury concentrations is due to the detection limit of the ICP-MS instrument of 0.02 μg/L given by the manufacturer. This rapid equilibration is enhanced not only by the affinity of thiol to mercury species but also by the hydrophilic character of the sorbent material. The relatively slower kinetics observed for the 50 mg/L solution are due to the system reaching equilibrium capacity.

Figure 4 shows the theoretical predictions of the experimental data using the film−pore and chemical reaction models. The two curves for $[Hg]_0$ of 5 and 0.5 mg/L for both the chemical reaction and film−pore models essentially overlap. An average particle diameter of 152 μm of the range 125−180 μm is used in the calculations, as determined from particle size distribution analysis of 500 particles using Scion Image version 4.0.2. The fitting parameters of the film−pore model, molecular diffusivity, D_M, and tortuosity, τ, are determined to be 5.6 × 10^{-6} cm^2/s and 2, respectively. In Table 5, the calculated results of the corresponding D_p value and the determined fitting parameter of the chemical reaction model, k_2, are summarized. The k_f values are not reported because they are large as a result of the high flow rate employed, and the corresponding bulk and surface concentrations are approximately the same. Quantitative evaluation of the two

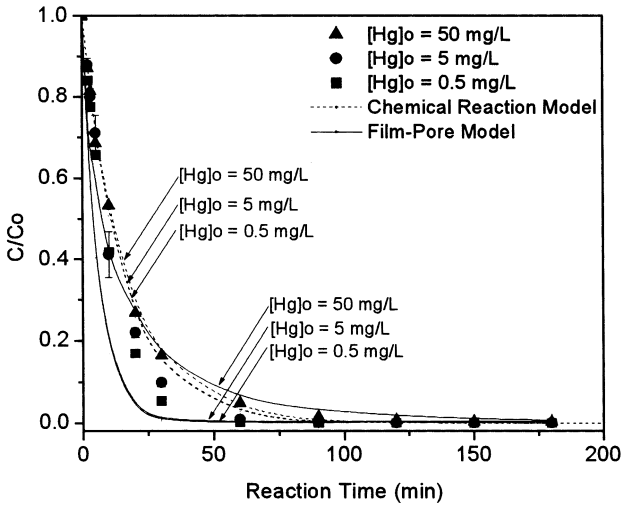

Figure 4. Adsorption kinetics modeling of mercury on SOL-AD-IV for different mercury concentrations.

Table 5. Kinetic Results of Film−Pore and Chemical Reaction Models

model	overall AARD[a]	D_p (cm^2/s)	k_2 (L/mmol·s)
film−pore	0.35	1.72×10^{-6}	
chemical reaction	0.50		0.399

[a] Calculated for $0 \le t \le 60$ min because of increased scattering of data after 60 min.

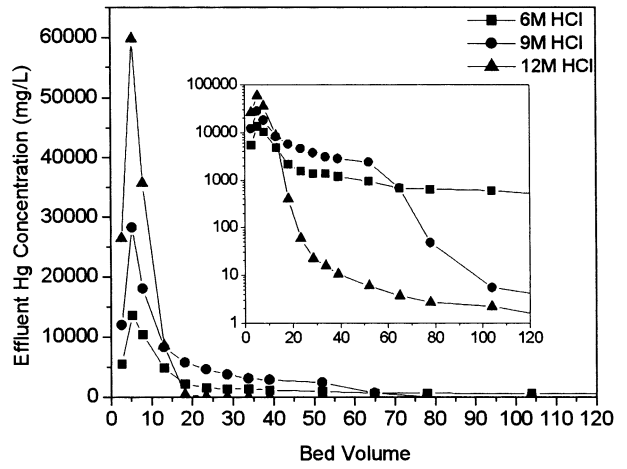

Figure 5. Stripping tests of mercury using various HCl concentrations: weight of SOL-AD-IV = 0.2 g; loading of SOL-AD-IV using 500 mL of a 400 mg/L Hg solution at pH 5.

models based on the overall absolute average relative deviation (AARD) error analyses suggests that the film−pore model predicts the experimental data better than the chemical reaction model. The AARD is defined as

$$\mathrm{AARD} = \frac{1}{n}\sum_{i=1}^{n}\left|\frac{C_{\mathrm{exp},i} - C_{\mathrm{calc},i}}{C_{\mathrm{exp},i}}\right| \qquad (19)$$

4.4. Stripping. Hydrochloric acid is typically used as the stripping agent in mercury studies.[8−11,23] Concentrated nitric and sulfuric acids are potential stripping agents also; however, because of their oxidizing capabilities, their use over adsorbents with thiol functional groups is not appropriate because of the potential loss of ligand functionality. Figure 5, presenting the stripping efficiencies of the three concentrations used (6, 9, and 12 M HCl), shows that the 12 M HCl solution is most efficient based on the amount of stripped mercury as a function of the bed volume. Specifically, at 8 bed volumes, 95% is stripped.

Table 6. Solubility Products of Metal Sulfides and Corresponding Extraction Efficiencies

metal[a]	pK_{sp}	% extraction	metal[a]	pK_{sp}	% extraction
Hg(II)	52.4	99.9	As(V)	∼21	22.1
Pb(II)	27.9	53.3	Cr(III)	NA	5.8
Cd(II)	26.1	51.9			

[a] Equimolar amounts (0.0744 mmol) of each metal in 1 L is used at pH_e 4.

Adsorbed mercury chloride and mercury acetate complexes may undergo the following stripping mechanisms:

$$\overline{\mathrm{RS{\cdot}HgCl}} + 3\mathrm{HCl} \leftrightarrow \overline{\mathrm{RSH}} + \mathrm{HgCl_4^{2-}} + 2\mathrm{H^+} \qquad (20)$$

$$\overline{\mathrm{RS{\cdot}HgAc}} + 4\mathrm{HCl} \leftrightarrow \overline{\mathrm{RSH}} + \mathrm{HgCl_4^{2-}} + \mathrm{Ac^-} + 3\mathrm{H^+} \qquad (21)$$

Protons replace adsorbed mercury complexes, thereby reactivating the sites to the thiol groups (−SH). The released mercury binds with chlorides to form $HgCl_4^{2-}$ as a result of the excessive chloride concentration. This divalent anionic mercury species is predominantly present at chloride concentrations greater than 1 M, as is indicated by speciation calculations using MINEQL+ and others.[3,12] The equilibria of mercury chloride complexes, shown in eq 1, shift to the right.

4.5. Selectivity. The selectivity of SOL-AD-IV for different hazardous metals [Hg(II), Cd(II), Pb(II), As(V), Cr(III)] is investigated and presented in Table 6 because these trace amounts in scrubber solutions have potential chelating properties with thiol groups. The selectivity of the adsorbent is found to decrease in the order Hg > Pb ∼ Cd > As > Cr and shows proportionality to pK_{sp} values. A study[50] conducted using a commercial thiol resin, Duolite GT-73, shows a relationship similar to that between percent extractions in multimetal adsorption and solubility products. It is implicative that, during column adsorption operations using real wastewaters, displacement of any adsorbed Pb, Cd, As, and Cr by the more selective Hg will take place because this behavior is observed by others.[10]

4.6. Breakthrough Curves. Dynamic adsorption is tested in fixed-bed operational schemes using high and low mercury feed concentrations because they are process efficient in terms of adsorbent utilization and regenerability. Breakthrough profiles are presented with theoretical predictions using the film−pore model for fixed-bed column adsorption.

The high mercury concentration breakthrough curve is shown in Figure 6. As expected, there is a release of protons upon adsorption, and upon saturation, the pH approaches the initial value. A comparison of the moles of protons released to the moles of mercury adsorbed indicates a ratio of 1.06 (0.611 mmol of Hg/0.579 mmol of H^+), which confirms the 1:1 complexation between mercury and thiol sites, according to the proposed mechanism of eq 6.

For the short column used (bed height = 1 cm), the length of the mass-transfer zone is estimated[51] to be around 0.3 cm based on the width of the breakthrough curve on the abscissa. Consequently, the fraction of the unused bed at breakthrough will be smaller in longer columns. The mercury capacity is determined to be 608

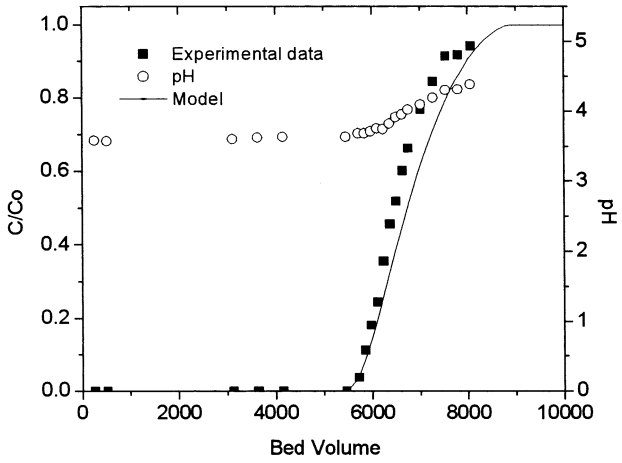

Figure 6. High-concentration breakthrough curve of mercury on a SOL-AD-IV bed with model prediction: 1 bed volume = 0.385 cm^3; $[Hg]_{feed}$ = 50 mg/L at pH 5; volume = 3.1 L; weight of SOL-AD-IV = 0.2 g; Q = 1.1 mL/min; saturation capacity = 608 mg/g.

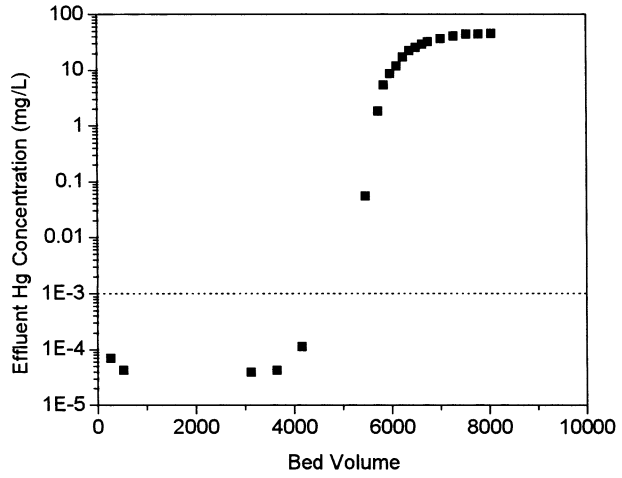

Figure 7. High-concentration breakthrough curve of mercury on a SOL-AD-IV bed showing effluent concentrations.

mg/g at saturation, which is close to the experimental equilibrium capacity of 680 mg/g, and 389 mg/g at the breakpoint ($[Hg]_{effluent} > 1\ \mu g/L$). This capacity indicates that 12 L of a 50 mg/L mercury solution can be treated with 1 g of SOL-AD-IV at saturation. To show the extent of removal efficiency, the effluent concentrations as a function of the bed volume are shown in Figure 7. It is evident from the figure that the goal of obtaining <1 μg/L (shown by the horizontal dotted line) in the effluent is clearly achieved, with an average concentration up to the breakpoint of 0.06 μg/L.

The prediction of the experimental data using the film−pore model is also shown in Figure 6. Because the model regards both film and pore diffusion as significant and thus controlling, evaluation of the actual controlling step is conducted by k_f and D_p sensitivity analyses. Although not reported here, results indicate that the model is more sensitive toward D_p than k_f, thereby implying that the adsorption of mercury on SOL-AD-IV is controlled by pore diffusion transport. The values of the calculated k_f and the corresponding Biot numbers, Bi, are shown in Table 7.

A second fixed-bed column adsorption test is conducted using low mercury concentrations to demonstrate the removal of mercury from scrubber composition solutions. A small adsorbent bed and a high flow

Table 7. Experimental Conditions and Results of Column Adsorption

$[Hg]_0$ (mg/L)	pH initial	q_{sat} (mg/g)	$q_{breakpoint}$[a] (mg/g)	Q (mL/min)	k_f (cm/s)	Bi
50	4.8	608	389	1.1	0.0124	54.1
0.5	5	391	150	6.0	0.0191	83.6

[a] Breakpoint occurs when $[Hg]_{effluent} > 1\ \mu g/L$.

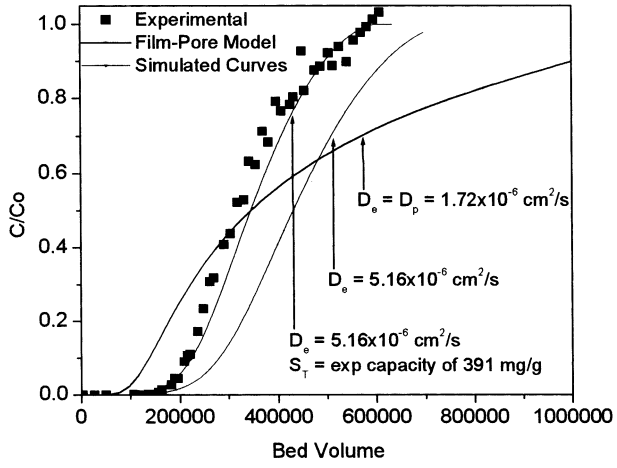

Figure 8. Low-concentration breakthrough curve of mercury on a SOL-AD-IV bed with model prediction and simulated curves: 1 bed volume = 0.327 cm^3; $[Hg]_{feed}$ = 0.5 mg/L at pH 5; volume = 205 L; weight = 0.175 g; Q = 6.0 mL/min; saturation capacity = 391 mg/g.

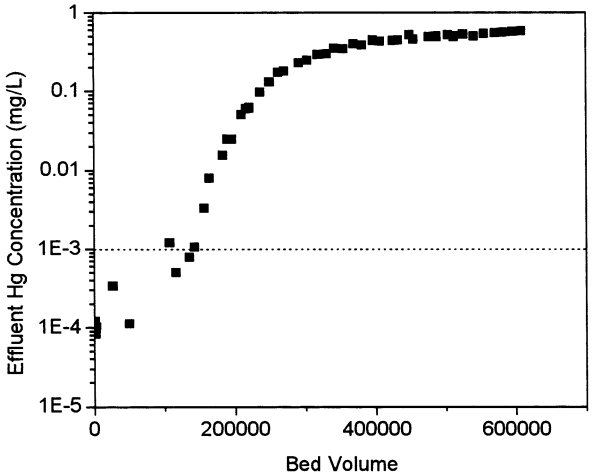

Figure 9. Low-concentration breakthrough curve of mercury on a SOL-AD-IV bed showing effluent concentrations.

rate are employed to avoid operation for extended periods of time and permit feasible laboratory experimentation. The breakthrough curve for the mercury feed solution concentration of 0.5 mg/L at pH 5 operated for 24 days is shown in Figure 8. The mercury capacity is calculated to be 391 mg/g at saturation and 150 mg/g at the breakpoint ($[Hg]_{effluent} > 1\ \mu g/L$), whereas the expected uptake capacity at saturation estimated from the equilibrium isotherm is 500 mg/g. This difference is thought to be a manifestation of deactivation and is discussed later in this section. Regardless, it is estimated that 782 L of a 0.5 mg/L mercury solution can be treated with 1 g of SOL-AD-IV at saturation. To determine the extent of removal of mercury from the scrubber simulant, the effluent concentrations are plotted in Figure 9, where it is shown that the effluent

Table 8. Comparison of Adsorbents for Mercury Extraction from Aqueous Solutions

material	q_{max} (mg/g)	surface area (m^2/g)	D (Å)	material support	ref
SOL-AD-IV	726[a] (1287[b])	540	70 (20−400)[c]	silica	this work
thiol-SAMMS	635	871	55 (15−400)[c]	silica	25
Duolite GT-73	363	47.3[d]	macroporous	polystyrene/divinylbenzene	3
Mg-MTMS	603	58	2.7	magnesium phyllosilicate clay	23

[a] q_{max} in chloride media; the adsorbing species is $HgCl_2^0$, revealing a 1:1 complexation ratio between the mercury species and thiol groups. [b] q_{max} in aqueous media,[36] revealing a 1.7:1 complexation ratio between mercury species and thiol groups. Speciation using MINEQL+ indicates that mercury exists predominantly as $Hg(OH)_2^0$ in the aqueous solution matrix; however, studies[41,49] indicate that mercury hydroxide may be present as polynuclear complexes, which can justify this complexation ratio. [c] Pore diameter distribution range provided in parentheses. [d] Reference 54.

concentrations are below 1 μg/L for 130 000 bed volumes (120 h).

The prediction of the experimental data using the film−pore model shown in Figure 8, represented by the solid line, indicates that the model does not describe the breakthrough data for this low mercury concentration system (0.5 mg/L Hg). This result suggests that additional resistances such as surface diffusion are present. Effective diffusivity, defined as

$$D_e = D_p + \rho_s D_s \frac{\delta q}{\delta C} \qquad (22)$$

takes into account the slope of the adsorption isotherm $\delta q/\delta C$ in the surface diffusion term. The increase in D_e with a decrease in the concentration is observed by McKay and Al-Duri[52] in nonlinear isotherms. They also indicated that D_e approaches D_p as the concentration increases. Similarly for this study, with the low concentration of 0.5 mg/L, $\delta q/\delta C$ becomes significant in the nonlinear isotherm (Figure 2), giving D_e a greater contribution from surface diffusion. One can experimentally determine when surface diffusion is important by plotting D_e versus the initial solution concentration and defining the region where D_e is nonlinear. For the 50 mg/L concentration case, $\delta q/\delta C$ is small, and hence the assumption that $D_e = D_p$ is valid. Thus, for this low concentration system, several D_e values are tested. The experimental data are better approximated using $D_e = 5.2 \times 10^{-6}$ cm^2/s ($3D_p$) as compared to using $D_e = D_p$ (1.7×10^{-6} cm^2/s). These results indicate that surface diffusion effects are significant for these low mercury concentrations. The enduring deviation of the simulated curve from the experimental data may be a result of deactivation of the thiol groups upon operation for 24 days. This loss of capacity is likely due to the oxidation of the thiol groups to disulfides, mercury ions themselves deactivating these groups, or mercury acting as a catalyst for thiol oxidation by nitrates.[6] The sorbents can be reactivated by treatment with 2-mercaptoethanol, which reduces disulfides to thiols.[6,53] A simulated breakthrough curve generated using the experimental capacity and the simulated D_e value of 5.16×10^{-6} cm^2/s predicts the experimental data well. The above results indicate that, during column operations using low mercury concentrations, surface diffusion is likely to be a contributing factor to diffusional resistances and that a long-term deactivation occurs. It is noted that the concentration region for which D_e is nonlinear can be experimentally determined by plotting D_e versus the initial solution concentration.

4.7. Stability. The results of the multiple adsorption/desorption cycle test to determine the chemical stability of thiol groups and the regenerability of SOL-AD-IV are shown in Figure 10. The capacity ratio, q_i/q_o, is plotted against the number of cycles of operation, where q_i is the mercury uptake after the ith cycle and q_o is that after the first cycle. The mercury adsorption capacity gradually decreases through 10 cycles and retains its capacity until the 25th cycle, corresponding to approximately 10% capacity loss from the initial capacity of 767 mg/g to 691 mg/g. The capacity loss may be due to irreversible mercury adsorption and/or oxidation of thiol groups. The results indicate that the thiol functional groups are chemically stable to 12 M HCl stripping solutions and that effective regeneration is achieved.

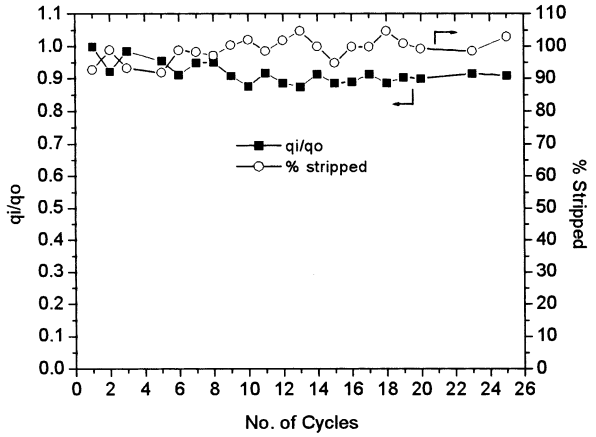

Figure 10. Stability test of SOL-AD-IV for multiple adsorption/desorption cycles: q_i is the mercury uptake after the ith cycle; q_o is the mercury uptake after the first cycle; loading with 1 L of a 300 mg/L Hg solution at pH 5; stripping with 25 mL of 12 M HCl.

4.8. Comparison to Other Thiol Materials. The mercury extraction performance of SOL-AD-IV is quantitatively compared with other sorbents, as shown in Table 8, by means of maximum mercury uptake capacities and material structural properties. Thiol-SAMMS, developed recently by the Pacific Northwest National Laboratory, is a thiol functional adsorbent targeted for mercury removal. It is reported that approximately 50% of the original mercury capacity is lost after one regeneration cycle (batch mode).[55] Duolite GT-73, a commercial ion-exchange resin developed by Rohm and Haas Co., has been used for the extraction of many heavy and noble metals including mercury. The maximum mercury capacity is less than half the value obtained in this study. Mg-MTMS is an adsorbent synthesized by co-condensation of organosiloxane and $MgCl_2$. The microscale of the pore seems unattractive because of the tendency of the adsorbing solutes to be larger than 3 or 4 Å. In addition, the surface area is an order of magnitude smaller than that of SOL-AD-IV, although the maximum mercury uptake capacities are similar. The most attractive characteristic of SOL-AD-IV is its ability to regenerate for an extended number of cycles without losing much of its original mercury

uptake capacity. It therefore shows potential applicability in the industrial treatments of mercury-contaminated waters.

5. Conclusion

The removal of mercury from scrubber solutions is effectively demonstrated by using the organoceramic adsorbent SOL-AD-IV. Adsorption equilibrium measurements indicate that the mercury uptake capacity at the scrubber solution composition (0.5 mg/L) is 500 mg/g and that at saturation is 726 mg/g (the highest so far found in the literature). Adsorption kinetic studies show that SOL-AD-IV removes mercury at a rapid rate. Adsorbent regeneration is effectively accomplished using concentrated hydrochloric acid solutions. The selectivity of SOL-AD-IV indicates a high affinity for mercury. Removal of mercury from the scrubber simulant is successfully demonstrated in a fixed-bed column by achieving less than 1 μg/L mercury concentration in the effluent. A stability test operated for 25 adsorption/desorption cycles indicates a high stability of SOL-AD-IV with <10% loss of its original capacity. These results show a high potential for application in mercury cleanup of scrubber waters and potentially other wastewaters, and, in particular, it is due to the high mercury uptake and long life cycle.

Economic analysis of the treatment process with the novel material SOL-AD-IV is currently being conducted. Analysis will also include disposal methods such as sulfide precipitation and cementation using metallic iron.

Acknowledgment

The financial support of U.S. EPA NRMRL through Grant GR828570-01-0 is gratefully acknowledged. We thank Professor Richard V. Calabrese and Mr. Gustavo A. Padron of the University of Maryland for providing particle images and guidance in the analysis.

Nomenclature

Ac = acetate ion, CH_3COO^-
Bi = Biot number, $R_p k_f/2D_p$
C = Hg concentration in the pore, mmol/L
C_b = Hg concentration of the bulk, mmol/L
C_{b0} = initial/feed Hg concentration of the bulk, mmol/L
C_{calc} = model concentration, mmol/L
C_{exp} = experimental concentration, mmol/L
C_s = Hg concentration at the pellet surface, mmol/L
C_T = Hg concentration in the feed tank, mmol/L
D_p = pore diffusivity, cm^2/s
D_M = molecular diffusivity, cm^2/s
I = ionic strength, mol/L
k_{-1} = reverse reaction rate constant
k_1 = forward reaction rate constant
K_{eq} = equilibrium constant
k_f = film coefficient, cm/s
L = length of the column bed, cm
M = weight of the adsorbent, g
n = number of experimental data points
q = local Hg concentration in the pellet, mmol of Hg/g of adsorbent
$\bar{q}$ = average Hg concentration in the pellet, mmol of Hg/g of adsorbent
r = radial direction of the pellet
R_p = radius of the pellet, cm
S_t = theoretical mercury capacity, mmol of Hg/g of adsorbent
t = time, min
u_s = superficial velocity
V = volume of the solution, L
V_R = reactor volume, L
V_T = feed tank volume, L
z = axial direction in the column

Greek Letters

γ = activity coefficient
μ = liquid viscosity, cP
ϵ_p = pellet porosity
ϵ_b = bed porosity
ρ_p = pellet density, g/cm^3
ρ_b = bed density, g/cm^3
ρ_s = solid density of the adsorbent, g/cm^3
θ = corrected time for column calculations, $t - z\epsilon/u_s$
τ = particle tortuosity

Literature Cited

(1) Kudlac, G. A.; Amrhein, G. T. Enhanced Mercury Control for Coal-Fired Utility Boilers; McDermott Technology Inc. Report MTI 00-24; 7th Annual Pittsburgh Coal Conference, Pittsburgh, PA, 2000.

(2) DeVito, M. S. *Mercury Emissions at FGD-Equipped Coal-Fired Utilities*; CONSOL Inc.: Library, PA, 1997.

(3) Ritter, J. A.; Bibler, J. P. Removal of Mercury from Waste Water: Large-Scale Performance of an Ion-Exchange Process. *Water Sci. Technol.* **1992**, *25*, 165.

(4) USEPA. *National Primary Drinking Water Standards*; Report EPA 816-F-01-007; EPA: Washington, DC, 2001.

(5) Ferreira, L. M.; De Carvalho, J. M. R. Mercury Removal from Chloro-Alkali Plant Waste Waters by Ion Exchange. *Environ. Technol.* **1997**, *18*, 443.

(6) Deratani, A.; Sebille, B. Metal Ion Extraction with a Thiol Hydrophilic Resin. *Anal. Chem.* **1981**, *53*, 1742.

(7) Chiarle, S.; Ratto, M.; Rovatti, M. Mercury Removal From Water by Ion Exchange Resins Adsorption. *Water Res.* **2000**, *34*, 2971.

(8) Monteagudo, J. M.; Ortiz, M. J. Removal of Inorganic Mercury from Mine Waste Water by Ion Exchange. *J. Chem. Technol. Biotechnol.* **2000**, *75*, 767.

(9) Sugii, A.; Ogawa, N.; Hashizume, H. Preparation and Properties of Macroreticular Resins Containing Thiazole and Thiazoline Groups. *Talanta* **1980**, *27*, 627.

(10) De Jong, G. J.; Rekers, C. J. N. The AKZO Process for the Removal of Mercury from Waste Water. *J. Chromatogr.* **1974**, *102*, 443.

(11) Dujardin, M. C.; Caze, C.; Vroman, I. Ion-exchange Resins Bearing Thiol Groups to Remove Mercury. Part 1: Synthesis and Use of Polymers Prepared from Thioester Supported Resin. *React. Funct. Polym.* **2000**, *43*, 123.

(12) Lauth, M.; Frere, Y.; Prevost, M.; Gramain, P. H. Complexation Properties of a Homologous Series of Linear Polythioethers Grafted onto Macroporous Polystyrene Matrices: Selective Binding of Mercury(II) and Silver(I). *React. Polym.* **1990**, *13*, 73.

(13) Kataoka, T.; Yoshida, H. Adsorption of $HgCl_2$ on Cl^- Form Anion Exchangers—Equilibrium Isotherm. *Chem. Eng. J.* **1988**, *37*, 107.

(14) Slovak, Z.; Smrz, M.; Docekal, B.; Slovakova, S. Analytical Behavior of Hydrophilic Glycolmethacrylate Gels with Bound Thiol Groups. *Anal. Chim. Acta* **1979**, *111*, 243.

(15) Anjaneyulu, Y.; Rao, R. V. S. Application of APDC Coupled Polyurethane Foam Sorbent for the Removal and Recovery of Toxic Heavy Metals Hg, Cd and Pb from Industrial Effluents. *Can. J. Chem. Eng.* **2001**, *79*, 71.

(16) Sevdic, D.; Meider, H. Solvent Extraction of Silver(I) and Mercury(II) by *O*,*O*-Di-*n*-butyl α-Phenylamino-Phenylmethanethio Phosphonate from Chloride Solutions. *Solvent Extr. Ion Exch.* **1990**, *8*, 643.

(17) Brewer, K. N.; Herbst, R. S.; Glagolenko, I. Y.; Todd, T. A. Mercury Extraction by the TRUEX Process Solvent. III. Extractable Species and Stoichiometry. *Solvent Extr. Ion Exch.* **1998**, *16* (2), 487.

(18) Fiskum, S. K.; Rapko, B. M.; Lumetta, G. J. Partitioning of Mercury from Actinides in the TRUEX Process. *Solvent Extr. Ion Exch.* **2001**, *19* (4), 643.

(19) Herbst, R. S.; Brewer, K. N.; Tranter, T. J.; Todd, T. A. Mercury Extraction by the TRUEX Process Solvent. I. Kinetics, Extractable Species, & Dependence on Nitric Acid Concentration. *Solvent Extr. Ion Exch.* **1995**, *13*, 431.

(20) Sato, T.; Ishikawa, I.; Nakamura, T. Liquid−Liquid Extraction of Silver(I) and Mercury(II) form Nitric Acid Solutions by Alkylsulfide. *Solvent Extr. Ion Exch.* **1983**, *1*, 541.

(21) Reddy, M. L. P.; Francis, T. Recent Advances in the Solvent Extraction of Mercury (II) with Calixarenes and Crown Ethers. *Solvent Extr. Ion Exch.* **2001**, *19*, 839.

(22) Heitzsch, O.; Gloe, K.; Stephan, H.; Weber, E. Liquid−Liquid Extraction of Ag(I), Hg(II), Au(III) and Pd(II) by Some Oligothia Macrocyclic Ligands Incorporating Aromatic and Heteroaromatic Subunits. *Solvent Extr. Ion Exch.* **1994**, *12*, 475.

(23) Lagadic, I.; Mitchell, M.; Payne, B. Highly Effective Adsorption of Heavy Metal Ions by a Thiol-Functionalized Magnesium Phyllosilicate Clay. *Environ. Sci. Technol.* **2001**, *35*, 984.

(24) Mohan, D.; Gupta, V. K.; Srivastava, S. K.; Chander, S. Kinetics of Mercury Adsorption from Wastewater Using Activated Carbon Derived from Fertilizer Waste. *Colloids Surf. A* **2001**, *177*, 169.

(25) Mattigod, S. V.; Feng, X.; Fryxell, G. E.; Liu, J.; Gong, M. Separation of Complexed Mercury from Aqueous Wastes Using Self-Assembled Mercaptan on Mesoporous Silica. *Sep. Sci. Technol.* **1999**, *34*, 2329.

(26) Kawamura, Y.; Yoshida, H.; Asai, S.; Tanibe, H. Breakthrough Curve for Adsorption of Mercury(II) on Polyaminated Highly Porous Chitosan Beads. *Water Sci. Technol.* **1997**, *35*, 97.

(27) Hayakawa, K.; Yamakita, H. Preparation of Mercaptoethylated Graft Fibers for Adsorption of Heavy Metal Ions. *J. Appl. Polym. Sci.* **1997**, *21*, 665.

(28) USEPA. *Aqueous Mercury Treatment*; Capsule Report EPA 625-R-97-004; EPA: Washington, DC, 1997.

(29) Patterson, J. W.; Passino, R. *Metals Speciation−Separation and Recovery*; Lewis Publishers: New York, 1990.

(30) Terashima, Y. Removal of Dissolved Heavy Metals by Chemical Coagulation, Magnetic Seeding, and High Gradient Magnetic Filtration. *Water Res.* **1986**, *20*, 537.

(31) Larson, K. A. Liquid Ion Exchange for Mercury Removal from Water over a Wide pH Range. *Ind. Eng. Chem. Res.* **1992**, *31*, 2714.

(32) Yu, M.; Tian, W.; Sun, D.; Shen, W.; Wang, G.; Xu, N. Systematic Studies on Adsorption of 11 Trace Heavy Metals on Thiol Cotton Fiber. *Anal. Chim. Acta* **2001**, *428*, 209.

(33) Pearson, R. G. Hard and Soft Acids and Bases, HSAB, Part I: Fundamental Principles. *J. Chem. Educ.* **1968**, *45*, 581.

(34) Biscarini, P.; Fusina, L.; Nivellini, G. D. Dissociation and Structure of Addition Compounds Between Thioethers and Mercury(II) Chloride. *Inorg. Chem.* **1971**, *10*, 2564.

(35) SenGupta, A. K.; Marcus, Y. *Ion Exchange and Solvent Extraction*; Mercel Dekker: New York, 2001; Vol. 14.

(36) Lee, J. S.; Gomes-Salazar, S.; Tavlarides, L. L. Synthesis of Thiol Functionalized Organo-Ceramic Adsorbent by Sol−Gel Technology. *React. Funct. Polym.* **2001**, *49*, 159.

(37) Smith, J. M. *Chemical Engineering Kinetics*, 3rd ed.; Chemical Engineering Series; McGraw-Hill Inc.: New York, 1981.

(38) Schecher, W. D.; McAvoy, D. C. *MINEQL+: A Chemical Equilibrium Modeling System*, Version 4.0; Environmental Research Software, Hallowell, ME, 1998.

(39) Smith, R. M.; Martell, A. E. *Critical Stability Constants*; Plenum Press: New York, 1976; Vol. 4.

(40) Ciavatta, L.; Grimaldi, M. Equilibrium Constants of Mercury(II) Choride Complexes. *J. Inorg. Nucl. Chem.* **1968**, *30*, 197.

(41) MacNaughton, M. G. Adsorption of Mercury(II) at the Solid−Water Interface. Ph.D. Dissertation, Stanford University, Stanford, CA, 1973.

(42) Morel, F. M. M.; Hering, J. G. *Principles and Applications of Aquatic Chemistry*; John Wiley & Sons: New York, 1993.

(43) Gomez-Salazar, S. Modeling of Cadmium Adsorption on Organo-Ceramic Adsorbents Containing the Thiol Group. Ph.D. Dissertation, Syracuse University, Syracuse, NY, 2002.

(44) Martell, A. E.; Smith, R. N. *Critical Stability Constants*; Plenum Press: New York, 1976; Vol. 5, Supplement I.

(45) *Microcal Origin*, Version 6.0; Mircrocal Software, Inc.: Northampton, MA, 1997.

(46) Tien, C. *Adsorption Calculations and Modeling*; Butterworths-Heinemann: Newton, MA, 1994.

(47) Schiesser, W. E. *The Numerical Method of Lines*; Academic Press Inc.: San Diego, CA, 1991.

(48) Seader, J. D.; Henley, E. J. *Separation Process Principles*; John Wiley & Sons: New York, 1998.

(49) Grdenic, D. The Structural Chemistry of Mercury. *Quart. Rev.* **1965**, *19*, 303.

(50) Choi, B. S.; Jung, H. S. A Study on the Adsorption Behavior of Some Heavy Metals on Duolite GT-73 Chelating Resin. *Bull. Korean Chem. Soc.* **2000**, *21*, 538.

(51) Wankat, P. C. *Rate-controlled Separations*; Elsevier Science: New York, 1990.

(52) McKay, G.; Al-Duri, B. Study of the Mechanism of Pore Diffusion in Batch Adsorption Systems. *J. Chem. Technol. Biotechnol.* **1990**, *48*, 269.

(53) Deratani, A.; Sebille, B. Preparation and Characterization of a Polyacrylamide Resin Containing Thiol Groups. Study of the Reversible Zn(II) Fixation. *Makromol. Chem.* **1981**, *182*, 1875.

(54) Saha, B.; Iglesias, M.; Cumming, I. W.; Streat, M. Sorption of Trace Heavy Metals by Thiol Containing Chelating Resins. *Solvent Extr. Ion Exch.* **2000**, *18* (1), 133.

(55) Feng, X.; Fryxell, G. E.; Wang, L.-Q.; Kim, A. Y.; Liu, J.; Kemner, K. M. Functionalized Monolayers on Ordered Mesoporous Supports. *Science* **1997**, *276*, 923.

Received for review October 23, 2002
Revised manuscript received January 29, 2003
Accepted February 6, 2003

IE020834L